

Manuscript Number:

Title: Nanopattern formation in UV laser treated a-AlO<sub>x</sub> and nc-Al/AlO<sub>x</sub> layers

Article Type: Full Length Article

Section/Category: Full Length Article

Keywords: nanopatterning; UV laser; Langmuir-Blodgett film; ordered nanostructures

Corresponding Author: Mr. János Szívós,

Corresponding Author's Institution: Institute for Technical Physics and Materials Science

First Author: János Szívós

Order of Authors: János Szívós; Miklós Serényi, DSc; Eszter Gergely-Fülöp; Tivadar Lohner, DSc; György Sáfrán, PhD

Abstract: Hexagonal nanopatterns were fabricated in sputter deposited Al-oxide thin films by means of single UV laser pulses via a layer of self-assembled silica nanospheres. The hexagonal pattern was projected to the surface due to the focussing effect of the silica nanolenses enhancing the local impact of the pulse. As a result of the laser pulse large area ordered structure of nano-pits were formed in RF sputtered amorphous Al-oxide films, while nano-craters were created in DC sputter deposited layers that consist of Al nanocrystals embedded in amorphous matrix. The two different mechanisms governing the nanostructure formation in the a-AlO<sub>x</sub> and nc-Al/AlO<sub>x</sub> composite layers were revealed by Atomic Force Microscopy (AFM), cross-sectional Transmission Electron Microscopy (XTEM), spectroscopic ellipsometry and computer simulation.

Suggested Reviewers: Ute Kaiser PhD, DSC

Electron Microscopy Group of Materials Science, University Ulm, Central Facility of Electron Microscopy  
ute.kaiser@uni-ulm.de

Anita Horváth PhD

Surface Chemistry and Catalysis Department, Hungarian Academy of Sciences, Centre of Energy Research  
anita.horvath@energia.mta.hu

### Highlights

- DC and RF sputtered  $\text{AlO}_x$  surfaces had been treated by a single UV laser pulse.
- Focusing effect of silica nanospheres of the Langmuir-Blodgett film was confirmed.
- Ordered pit, or ordered hillock and crater patterns of 200 nm size were fabricated.
- Preparing nanostructures with periods below 100 nm is possible with this technique.
- The method enables the direct patterning of various materials.

## **Nanopattern formation in UV laser treated a-AlO<sub>x</sub> and nc-Al/AlO<sub>x</sub> layers**

**János Szívós<sup>1,2,\*</sup>, M. Serényi<sup>1</sup>, E. Gergely-Fülöp<sup>1</sup>, T. Lohner<sup>1</sup>, G. Sáfrán<sup>1</sup>**

<sup>1</sup>Institute for Technical Physics and Materials Science, Research Centre for Natural Sciences, Hungarian Academy of Sciences, H-1121 Budapest, Konkoly-Thege M. út 29–33.

<sup>2</sup>Doctoral School of Molecular- and Nanotechnologies, University of Pannonia, H-8200 Veszprém, Egyetem utca 10.

\*Corresponding author, e-mail: [szivos.janos@ttk.mta.hu](mailto:szivos.janos@ttk.mta.hu), phone: +36-1-392-2222/1876

### **Abstract**

Hexagonal nanopatterns were fabricated in sputter deposited Al-oxide thin films by means of single UV laser pulses via a layer of self-assembled silica nanospheres. The hexagonal pattern was projected to the surface due to the focussing effect of the silica nanolenses enhancing the local impact of the pulse. As a result of the laser pulse large area ordered structure of nano-pits were formed in RF sputtered amorphous Al-oxide films, while nano-craters were created in DC sputter deposited layers that consist of Al nanocrystals embedded in amorphous matrix. The two different mechanisms governing the nanostructure formation in the a-AlO<sub>x</sub> and nc-Al/AlO<sub>x</sub> composite layers were revealed by Atomic Force Microscopy (AFM), cross-sectional Transmission Electron Microscopy (XTEM), spectroscopic ellipsometry and computer simulation.

### **Keywords**

nanopatterning; UV laser; Langmuir-Blodgett film; ordered nanostructures

### **1 Introduction**

Nano-scale modification of various materials received wide research interest in the recent decades. This includes nanopatterning i.e. the preparation of nano size ordered structures. They are applied in the fields of tissue engineering [1], nanoelectromechanical systems (NEMS) [2], photonic crystals e.g. [3], [4], self-cleaning structures [5], and meta-materials [6], [7]. New type semiconductor devices can be developed

and the performance of conventional semiconductor devices can be improved with the help of nanopatterning [8]. The remarkable efforts to develop the bit patterned magnetic media (BPM) boost the improvement of various nanopatterning techniques. There are several techniques for the fabrication of ordered nanostructures [9], such as e-beam lithography [10], nanoimprinting [11], focused ion beam lithography (FIB) [12] and extreme ultraviolet lithography [13], or X-ray lithography [14]. Beside the above top-down techniques the bottom-up techniques are mainly based on nanosphere lithography [15] and molecular self-assembly [16]. Almost all processes mentioned above require selective (chemical) etching that may suffer from high costs and low throughput and the waste of the process is hazardous to nature.

In this paper a fast and low-cost method is proposed that is suitable to obtain ordered nanopatterns directly, or via preparation of Al-oxide masks and imprint molds for nanolithography. The technique does not involve chemical etching. A monolayer of self-assembled silica nanospheres prepared by the Langmuir-Blodgett (LB) technique [17], [18] is applied. The array of nanospheres is a template for a single pulse UV laser treatment of the surface. The laser treatment can be carried out either in vacuum or under atmospheric conditions. The treatment of relatively large areas requires only a single laser pulse that has 30 ns length.

Aluminium-oxide is a hard, durable, non-reactive, high melting-point material and it can be applied as (negative or positive) mask for nanolithography and as mold for nanoimprinting [19]. We have found earlier [20] that aluminium-oxide layers prepared by different techniques may behave differently under the UV laser treatment. The subject of this work is to compare the nanostructures formed in RF and DC sputtered Al-oxide subjected to laser pulses via self organized silica nanospheres and to reveal the different mechanisms that govern the nanostructure formation in a- $\text{AlO}_x$  and nc-Al/ $\text{AlO}_x$  composite layers.

## 2 Material and methods

$\text{AlO}_x$  layers were RF sputter deposited from a high purity alumina target with a minimum purity of 99.8% onto single crystal Si substrates. The films were deposited at room temperature at a rate of 0.25

Å/s. The base pressure of the vacuum chamber was below  $2 \times 10^{-6}$  mbar. The sputtering gas was an Ar – O<sub>2</sub> mixture with the partial pressures of  $1.6 \times 10^{-2}$  mbar and  $4 \times 10^{-3}$  mbar, respectively.

DC sputter deposited AlO<sub>x</sub> layers were prepared from an Al target (Aldrich 99.999) onto Si substrates at a base pressure of  $3 \times 10^{-5}$  mbar. The deposition was carried out at room temperature; the sputtering gas was a mixture of O<sub>2</sub> – Ar with partial pressures of  $4 \times 10^{-4}$  mbar and  $5 \times 10^{-3}$  mbar, respectively.

The deposited layers were covered with a monolayer of silica nanospheres self-organized in a hexagonal structure by the LB technique. The silica nanoparticles of 300 nm diameter and their LB-films were prepared as reported earlier [21], [22]. The LB-films were obtained using a KSV 2000 film balance by vertical deposition (5 mm/min) at cca. 80 % of the collapse pressure, which was determined in an earlier experimental run. After drying at 50°C in air, each samples covered with LB-film was exposed to a single pulse of a Kr-F UV excimer laser ( $\lambda=248$  nm).

In order to ensure acceptably uniform patterns, the intensity distribution of the laser spot was mapped prior to the treatments. A plan-parallel quartz plate that reflects ~4 % of the incoming intensity was exposed to the laser pulses so the reflected intensity could be measured indirectly with a GaP UV-photodiode. The intensity distribution was measured by scanning the photodiode stepwise across the spot (about 50x12 mm<sup>2</sup> size), with 1 mm<sup>2</sup> area resolution and recording the response voltage by an oscilloscope triggered with the laser pulses. The energy of the laser pulse was adjusted to  $100 \pm 6$  mJ, the pulse length was 30 ns, so the total power of each pulse was  $3.33 \pm 0.2$  MW. The current response of the photodiode is proportional to the power of the pulse; therefore the response signal integrated for the entire spot gave the total power of the mapped pulse.

During the patterning experiments the total energy of the pulse was varied between 75-105 mJ/pulse. Each sample was treated with a single shot of 30 ns pulse length. Repeated pulses would have hit the surface via silica nanospheres altered by the previous pulse and would deteriorate the quality of the pattern. After the laser treatment the LB-films were removed from the samples by acetone, in a frequency swept ultrasonic bath.

The structure and morphology of the samples were characterized by Atomic Force Microscopy (AFM) with an AIST-NT SmartSPM 1010 microscope, and Transmission Electron Microscopy (TEM) by means

of a 300kV JEOL 3010 (0.17 nm point resolution) and a 200 kV Philips CM 20 (0.27 nm point resolution) microscope. The preparation of the samples for TEM was carried out by mechanical and ion beam thinning. The penetration process of laser light at our experimental conditions was computer simulated with Crystalwave (<http://www.photond.com/products/crystalwave.htm>). A Woollam M-2000DI rotating compensator spectroscopic ellipsometer was applied to obtain the refractive index ( $n$ ) and absorption coefficient ( $\alpha=4\pi k/\lambda$ , where  $k$  is the extinction coefficient) of our layers.

### 3 Results

#### 3.1 Properties of the laser spot

As exposed from the measurements the UV laser spot shows a Gaussian-like intensity distribution plotted in the map in Fig. 1. Obviously, more than 14 kW is distributed in an area of 1 mm<sup>2</sup> at the most intense part of the spot while the power rapidly drops to 1-2 kW/mm<sup>2</sup> at the outer regions. For a fabrication of reasonably uniform patterns the inner part (5x9 mm<sup>2</sup>) of the spot was selected, as marked with a rectangle in the map, (inset of Fig. 1) and the outer regions were masked out. The total energy of the laser pulse was varied between 75±2 mJ and 105±2 mJ. These correspond to fluencies between 27±0.7 mJ/cm<sup>2</sup> and 38±0.7 mJ/cm<sup>2</sup> respectively. Here the intensity distribution of the entire spot was taken into account.

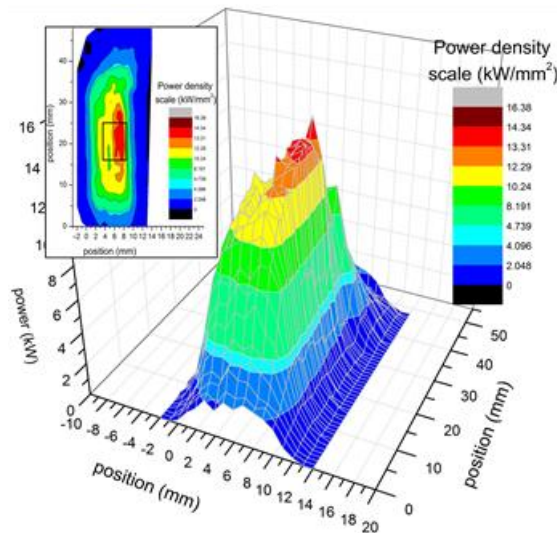


**Figure 1.** 3D image of the measured intensity distribution of the laser spot. Inset: top view color map of the spot. The effective part of the spot that passes through the aperture is marked with the black rectangle.

### 3.2 Results of the simulations

The incoming laser intensity was estimated to be homogenous in our computer simulations. In addition to the wavelength (248 nm) the simulation requires further parameters, namely, refractive index ( $n=1.681\pm0.005$ ) and absorption coefficient ( $\alpha=(3.86\pm0.15)\cdot10^4\text{ cm}^{-1}$ ). These parameters were taken from the data obtained by ellipsometry.

The silica particles of the LB-film focus the incoming laser light as individual spherical lenses - as it is seen in the computer simulated intensity distribution pattern (Fig. 2). Accordingly, the fluence of the laser light increases with an order of magnitude within the oxide layer, at the focus of the silica nanolenses (inset of Fig. 2). This occurs beneath every single silica nanosphere. The local modification of the alumina layer and the formation of ordered nanoscale patterns are based on this phenomenon.

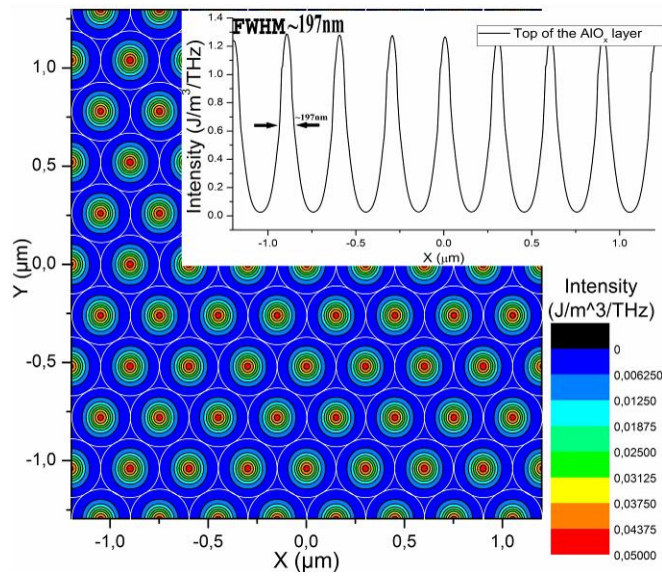


**Figure 2.** Focussing effect of the LB-film of silica nanospheres: simulated lateral intensity map. The intensity scales up from blue to red color. Inset: Simulated intensity profile at the top of the AlO<sub>x</sub> layer.

### 3.3 DC and RF sputtered AlO<sub>x</sub> films

The TEM investigations showed that Al-oxide layers prepared by RF sputtering are amorphous AlO<sub>x</sub> (a-AlO<sub>x</sub>), while the DC sputtered ones contain Al nanocrystals embedded in an amorphous Al-oxide matrix (nc-Al/AlO<sub>x</sub>). The structure and morphology of the a-AlO<sub>x</sub> and nc-Al/AlO<sub>x</sub> layers are represented in the TEM micrographs and Selected Area Electron Diffraction (SAED) patterns shown in Fig.3 a and b,

respectively. The diffuse rings in the SAED inset in Fig. 3 a represents a completely amorphous structure, while additional rings of embedded nanocrystalline Al can be recognized in the SAED in Fig. 3 b.

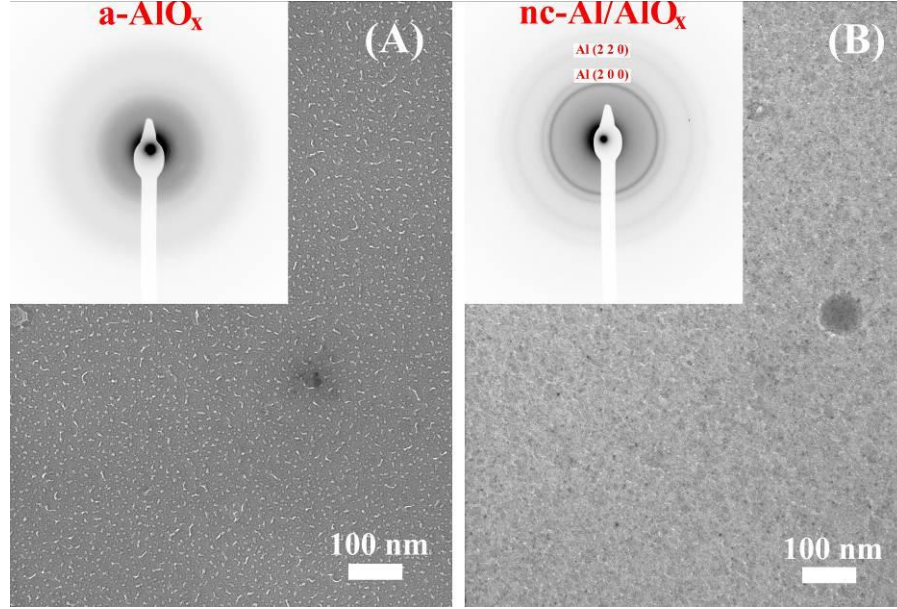


**Figure 3.** Plan view TEM images of the RF sputtered layers (a) and the DC sputtered ones (b). The SAED insets represent exclusively amorphous structure and amorphous with embedded Al nanocrystals, respectively.

The absorption coefficient ( $\alpha$ ) and refractive index curves obtained by ellipsometry measurements on the a-AlO<sub>x</sub> and on the nc-Al/AlO<sub>x</sub> are shown in Fig.4 a and b, respectively. Optical models were created with the input information that was found by TEM. It is to mention that the absorption coefficient ( $\alpha$ ) of the nc-Al/AlO<sub>x</sub> at  $\lambda=248$  nm is about 3 times higher than that of the a-AlO<sub>x</sub>.

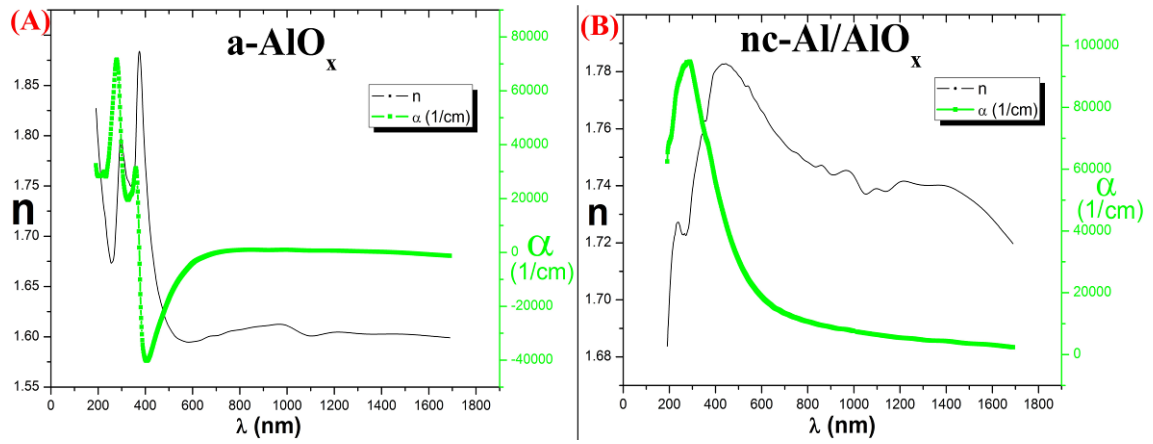


**Figure 4.** Refractive index ( $n$ ) and absorption coefficient ( $\alpha$ ) of a-AlO<sub>x</sub> (a) and nc-Al/AlO<sub>x</sub> (b) films as a function of wavelength.



### 3.4 Nanopatterns formed in a-AlO<sub>x</sub> layers

AFM investigation of RF sputtered a-AlO<sub>x</sub> films revealed uniform, hexagonal structure of shallow pits formed by the laser treatment. The images and corresponding depth profiles are shown in Fig. 5. The fluences of the laser shots were 27 mJ/cm<sup>2</sup>, 31 mJ/cm<sup>2</sup> and 38 mJ/cm<sup>2</sup> as depicted in Fig. 5 a, b, and c, respectively. At a fluence of 27 mJ/cm<sup>2</sup> the AFM-measured lateral size of the pits was 220±30 nm with the depth of 0.8±0.3 nm. The patterned surface and the wall of the pits is quite rugged represented by the image in Fig. 5 a, and by the corresponding depth profile in Fig. 5 d. The sample treated with an optimum fluence of 30 mJ/cm<sup>2</sup> showed 1.3±0.2 nm deep pits, while the walls and the surface of the pits were flat and uniform (Fig. 5 b and d). At the highest fluence 38 mJ/cm<sup>2</sup> a poor quality pattern shows up (c and d). The pits are non-uniform, most of them tend to coalesce and their depth decreases below 1 nm.

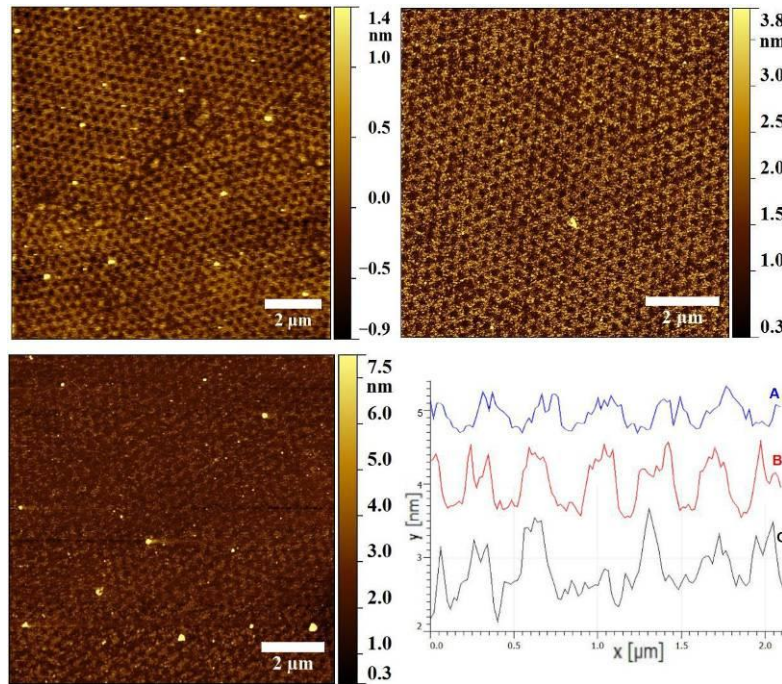


**Figure 5.** AFM results of the patterns obtained in a-AlO<sub>x</sub> by a single laser pulse at various fluences (~6x6 µm<sup>2</sup> area). The images of the samples prepared at fluence of 27±0.7 mJ/cm<sup>2</sup>, 30±0.7 mJ/cm<sup>2</sup>, and 38±0.7 mJ/cm<sup>2</sup> (~5x5 µm<sup>2</sup> area) are shown in (a), (b), and (c), respectively. The corresponding depth profiles are depicted in (d).

The cross-sectional TEM (XTEM) image of the a-AlO<sub>x</sub> layer treated with a pulse of fluence near to optimum (35 mJ/cm<sup>2</sup>) is shown in Fig. 6. A typical pit is seen here that exhibits about 220 nm diameter and 3-4 nm depth. A crystallized region of 15-20 nm width appears in the amorphous alumina at the

bottom of the pit that may indicate a heating effect of the pulse. The lateral size of the pit measured by XTEM fits well to the ones measured by AFM, while the depth is larger than shown by AFM.

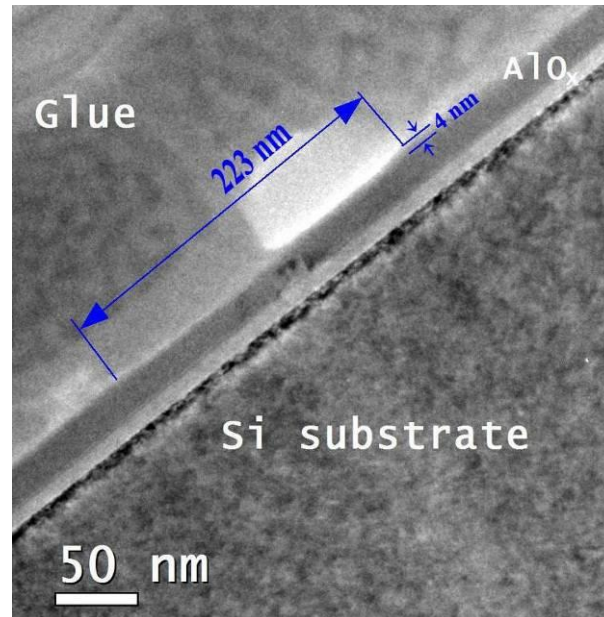


**Figure 6.** A cross-sectional TEM image of an  $\alpha$ - $\text{AlO}_x$  sample treated with  $35 \pm 0.7 \text{ mJ/cm}^2$  fluence. A typical pit is seen here, of  $\sim 200 \text{ nm}$  width and  $4 \text{ nm}$  depth. A crystallized area is recognized in the  $\text{AlO}_x$  beneath the centre of the pit.

The most regular pit pattern was found in samples treated with fluences about  $31 \text{ mJ/cm}^2$  (Fig 5 b). At this condition uniform patterns of  $200 \text{ nm}$  size pits were fabricated in domains that extend at least to  $250 \times 250 \mu\text{m}^2$  area (Fig. 7).

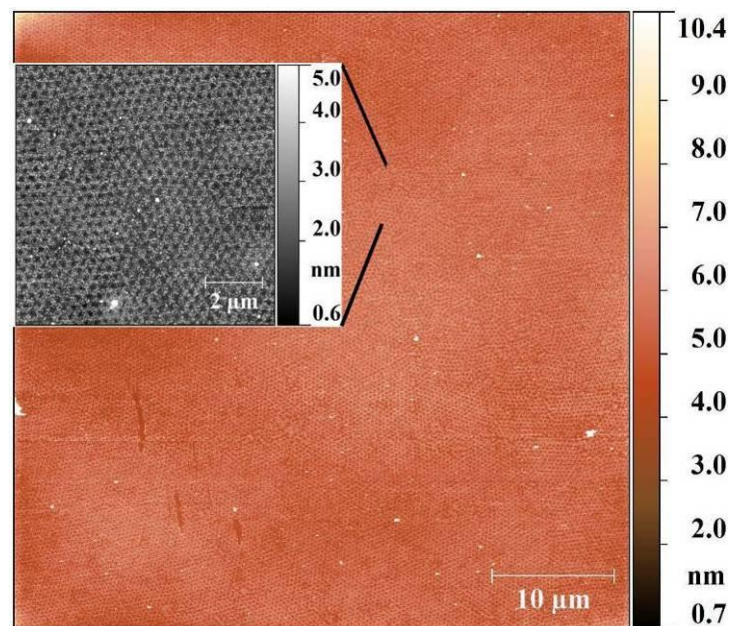


**Figure 7.** AFM image of an a-AlO<sub>x</sub> sample prepared at 30±0.7 mJ/cm<sup>2</sup> laser fluence, demonstrating the size (at least 80x80 μm<sup>2</sup>) of a patterned area. The arrangement and perfection of the pit pattern is directly related to that of the applied layer of silica nanospheres. Inset: a magnified ~9x9 μm<sup>2</sup> area.

### 3.5 Nanopatterns formed in nc-Al/AlO<sub>x</sub>

After laser-treatment of the samples the morphology of DC sputtered alumina layers with embedded Al nanocrystals proved to be remarkably different from that of amorphous alumina prepared by RF.

Depending on the local laser fluences hexagonal patterns of small and large hillocks (bubbles), and burst bubbles (craters) were observed by AFM. A ~30x30 μm<sup>2</sup> area with self organized features, typically burst bubbles are shown in Fig. 8 (average fluence ~32 mJ/cm<sup>2</sup>).

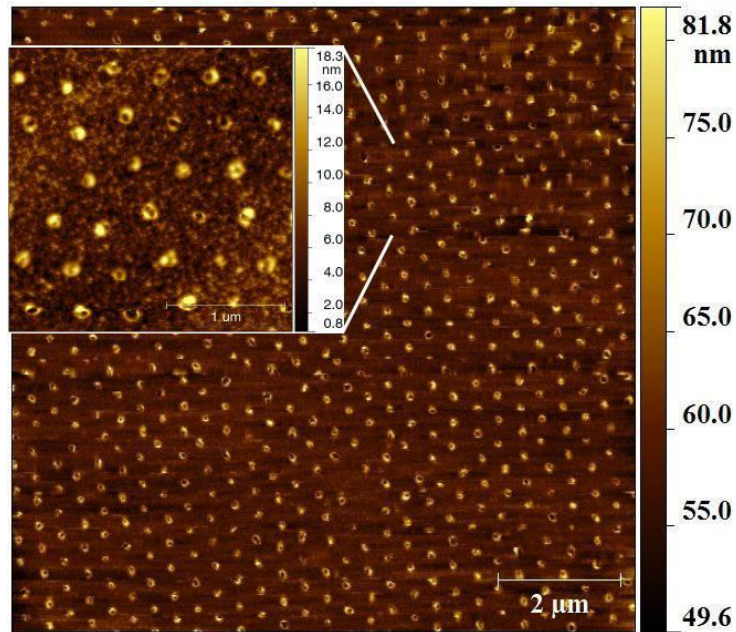


**Figure 8.** AFM image of a pattern of hillocks, bubbles and burst bubbles obtained at a fluence of 32 mJ/cm<sup>2</sup> in a nc-Al/AlO<sub>x</sub> film. Inset: a magnified ~2.5x2.5 μm<sup>2</sup> area.

In order to study the morphology of the above patterns in detail, the sample shown in Fig. 8 was investigated by cross-sectional TEM. The revealed morphologies are shown in Fig. 9. The image in (a) represents the side view of a hillock that was formed at the focal point of a silica nanosphere at a moderate local fluence. It contains both nanocrystals and small, distinct bubbles that make a local volume increase in the nc-Al/AlO<sub>x</sub> layer. Fig. 9 b shows a large, blown-up bubble with closed shell developed due to a slightly increased fluence. Further increase of the laser intensity caused the burst of the bubble

leaving behind a crater as depicted by Fig. 9 (c). The lateral extension and the depth of this crater is about 200 nm and 50 nm, respectively. This feature refers to the burst bubbles typical in the AFM image in Fig. 8.

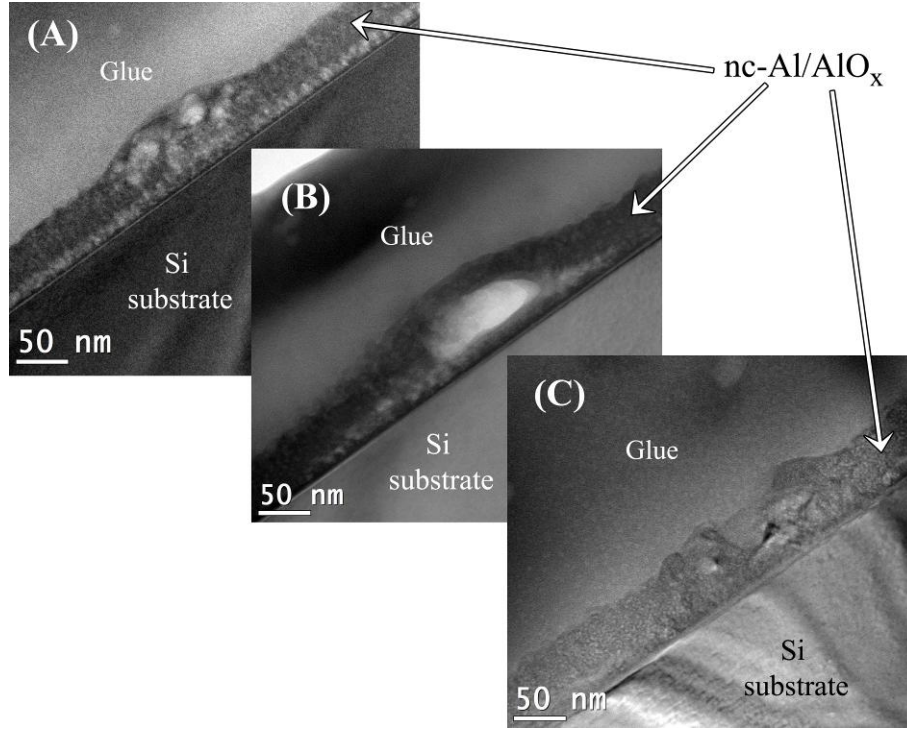


**Figure 9.** Side view TEM images of a hillock (a), a blown up bubble (b) and a burst bubble (crater) (c) formed in nc-Al/AlO<sub>x</sub> layers at the focal points of silica nanospheres under slightly increasing laser fluences. The average fluence was 32 mJ/cm<sup>2</sup>.

#### 4 Discussion

It was found that hexagonal nano-patterns with different morphologies can be prepared in RF and DC sputtered Al-oxide layers by means of single laser pulses using the focussing effect of self-assembled silica nanospheres. Since the size of the nanospheres (~300 nm) is larger than the wavelength of the illuminating laser (~248 nm), each sphere acts as an individual spherical lens and focuses the incoming laser light to the Al-oxide layer beneath. The simulated intensity distribution beneath a nanosphere shows around 200 nm full width at half maximum that is in a good agreement with the measured size of the formed features. The impact of the UV laser pulse highly depends on the optical properties of the treated layer. The low absorption coefficient of the a-AlO<sub>x</sub> suggests low energy deposit and heating effect in the RF sputtered samples at the focus of the nanospheres. In the DC sputtered nc-Al/AlO<sub>x</sub> films, however, the



3-times larger UV absorption causes significant energy deposit, heating and vapour release at the focal point of the silica nanospheres. These suggest different mechanisms for the formation of the patterns in the a-AlO<sub>x</sub> and the nc-Al/AlO<sub>x</sub> layers.

#### 4.1 Pit formation in a-AlO<sub>x</sub>

The shallow depth of the pits may be the consequence of the relatively low absorption coefficient ( $\alpha = (3.86 \pm 0.15) \times 10^4 \text{ cm}^{-1}$ ) of the amorphous AlO<sub>x</sub>. The calculated intensity drop of the passing light is only  $9.2 \pm 0.7 \%$ , therefore the energy deposited in the layer is relatively low. It evokes only restrained crystallization of the AlO<sub>x</sub> at the bottom of the pits (Fig. 6). The pit formation, however, cannot be explained by only the volume change due to amorphous to crystalline transition localized to 10-20 nm area. We suggest a restructuring with the contribution of nanovoids that are typical in amorphous materials: their inner surfaces are decorated and stabilized by electrically active dangling bonds [23]. Due to the shock wave of the electromagnetic field of the laser pulse the nanovoids collapse that results in a volume decrease, therefore, the formation of the shallow pits. This is a weak effect compared to the high energy provided by the laser pulse, however, it creates well recognizable intrinsic surface features.

#### 4.2 Crater formation in nc-Al/AlO<sub>x</sub>

In the highly absorbent nanocrystalline nc-Al/AlO<sub>x</sub> composite, significant UV energy is absorbed at the focal point of the silica nanolenses. The in-focus condensed energy is supposed to melt and evaporate the low melting point Al nanocrystals. The surrounding amorphous oxide may melt, simultaneously, and partly crystallizes on cooling. The Al-vapour evokes small, distinct bubbles and the additional volume forms protruding hillocks in the layer. At increasing laser fluences the small bubbles coalesce into single large bubbles that finally burst and create craters.

### 5 Conclusions

Ordered nanoscale patterns of ~200 nm lateral feature size were fabricated in RF and DC sputtered Al-oxide films by means of single laser pulses via a layer of self-assembled silica nanospheres. Hexagonally arranged patterns were prepared within domains as large as  $250 \times 250 \mu\text{m}^2$ , however, imperfections of the

LB-film were replicated into the pattern. Two different mechanisms are proposed for the nanopattern formations in amorphous alumina and in nanocrystalline Al/amorphous alumina composite layers. In case of low light-absorbance  $\alpha\text{-AlO}_x$  the heating effect of laser pulse is marginal. Therefore, pit formation at the focus of silica nanolenses is suggested to occur due to the collapse of dangling bonds-stabilized nanovoids under the electromagnetic shock wave of the laser pulse. In high absorbance nc-Al/amorphous alumina composite, however, the in-focus absorbed UV energy is supposed to melt and evaporate the Al nanocrystals and in addition it may melt and crystallize a part of the amorphous oxide. The vapour evokes small, distinct bubbles and the volume increase forms hillocks in the layer. At slightly higher fluences of the laser pulse the small bubbles coalesce into large bubbles that burst and create craters. This work suggests that the present technique is suitable for direct nanopatterning, as well fabrication of durable  $\text{AlO}_x$  imprint molds and masks for nanostructuring various surfaces. It is also an important issue that these nanostructures are fabricated environmentally friendly way, without chemical etching.

## 6 Acknowledgement

The authors are thankful to B. Fodor for ellipsometry measurements, to P. B. Barna and L. Tóth for valuable discussions. The contribution of Z. Szabó in the computer simulation is acknowledged. This work was partially supported by the National Development Agency grant TÁMOP-4.2.2/B-10/1-2010-0025.

## 7 References

- [1] Kim H N, Jiao A, Hwang N S, Kim M S, Kang D H, Kim D-H, et al. Nanotopography-guided tissue engineering and regenerative medicine. *Adv. Drug Deliver. Rev.* 2013;65(4):536–558.
- [2] Bhushan B. Nanotribology and nanomechanics of MEMS/NEMS and BioMEMS/BioNEMS materials and devices. *Microelectron. Eng.* 2007;84(3):387–412.
- [3] Tamáska I, Dobrik G, Nemes-Incze P, Kertész K, Horváth E, Márk G I, et al. *Thin Solid Films.* 2011;519(12):4078–4081.

- [4] Meng X, Gomard G, El Daif O, Drouard E, Orobtcouk R, Kaminski A, et al. Absorbing photonic crystals for silicon thin-film solar cells: Design, fabrication and experimental investigation. *Sol. Energ. Mat. Sol. C.* 2011;95 Suppl 1:S32–38.
- [5] Fürstner R, Barthlott W, Neinhuis C, Walzel P. Wetting and Self-Cleaning Properties of Artificial Superhydrophobic Surfaces. *Langmuir.* 2005;21:956-961.
- [6] Sihvola A, Metamaterials in electromagnetics. *Metamaterials.* 2007;1(1):2–11.
- [7] Boltasseva A, Shalaev V M. Fabrication of optical negative-index metamaterials: Recent advances and outlook. *Metamaterials.* 2008;2(1):1–17.
- [8] Zhao Q T, Klinkhammer F, Dolle M, Kappius L, Mantl S. A novel silicide nanopatterning method for the fabrication of ultra-short channel Schottky-tunneling MOSFETs. *Microelectron. Eng.* 2000;50(1–4):133–138.
- [9] Terris B D, Thomson T. Nanofabricated and self-assembled magnetic structures as data storage media. *J. Phys. D: Appl. Phys.* 2005;38:R199-222.
- [10] Noh J-S, Kim H, Chun D W, Jeong W Y, Lee W. Hyperfine FePt patterned media for terabit data storage. *Current Appl. Phys.* 2011;11(4 Suppl 1):S33–35
- [11] Chou S Y, Krauss P R, Renstrom P J. Imprint of sub-25 nm vias and trenches in polymers. *Appl. Phys. Lett.* 1995;67:3114-3116.
- [12] van Kan J A, Sanchez J L, Xu B, Osipowicz T, Watt F. Micromachining using focused high energy ion beams: Deep Ion Beam Lithography. *Nucl. Instrum. Meth. B.* 1999;148(1–4):1085-1089.
- [13] Gwyn C W, Stulen R, Sweeney D, Attwood D. Extreme ultraviolet lithography. *J. Vac. Sci. Technol. B.* 1998;16:3142-3149.
- [14] Heuberger A. X-ray lithography. *Microelectron. Eng.* 1986;5(1–4):3-38.
- [15] Haynes C L, Van Duyne R P. Nanosphere lithography: A versatile nanofabrication tool for studies of size-dependent nanoparticle optics. *J. Phys. Chem. B.* 2001;105:5599-5611.
- [16] Whitesides G M, Mathias J P, Seto C T. Molecular self-assembly and nanochemistry: a chemical strategy for the synthesis of nanostructures. *Science.* 1991;254(5036):1312-1319.
- [17] Stöber W, Fink A, Bohn E. Controlled growth of monodisperse silica spheres in the micron size range. *J. Colloid Interf. Sci.* 1968;26:62-69.
- [18] Schwartz D K. Langmuir-Blodgett film structure. *Surf. Sci. Rep.* 1997;27(7–8):245–334.

- [19] Jay Guo L. Nanoimprint lithography: methods and material requirements. *Adv. Mater.* 2007;19(4):495-513.
- [20] Rachel, Reinhard, editors. Nanoscale masking with UV excimer laser for bit patterned media. Proceedings of MC 2013; 2013 Aug 25-30; Regensburg, Germany. Regensburg: Unspecified; 2013.
- [21] Deák A, Hild E, Kovács A L, Hórvölgyi Z. Contact angle determination of nanoparticles: film balance and scanning angle reflectometry studies. *Phys. Chem. Chem. Phys.* 2007;9:6359-6370.
- [22] Deák A, Bancsi B, Tóth A L, Kovács A L, Hórvölgyi Z. Complex Langmuir–Blodgett Films from Silica Nanoparticles: An Optical Spectroscopy Study. *Colloid. Surface. A* 2006;278(1-3):10-16.
- [23] Bruno E, Mirabella S, Priolo F, Napolitani E, Bongiorno C, Raineri V. He induced nanovoids for point-defect engineering in B-implanted crystalline Si. *J. Appl. Phys.* 2007;101(2):023515

## 8 Figure Captions

**Figure 1.** 3D image of the measured intensity distribution of the laser spot. Inset: top view color map of the spot. The effective part of the spot that passes through the aperture is marked with the black rectangle.

**Figure 2.** Focussing effect of the LB-film of silica nanospheres: simulated lateral intensity map. The intensity scales up from blue to red color. Inset: Simulated intensity profile at the top of the  $\text{AlO}_x$  layer.

**Figure 3.** Plan view TEM images of the RF sputtered layers (a) and the DC sputtered ones (b). The SAED insets represent exclusively amorphous structure and amorphous with embedded Al nanocrystals, respectively.

**Figure 4.** Refractive index ( $n$ ) and absorption coefficient ( $\alpha$ ) of a- $\text{AlO}_x$  (a) and nc-Al/ $\text{AlO}_x$  (b) films as a function of wavelength.

**Figure 5.** AFM results of the patterns obtained in a- $\text{AlO}_x$  by a single laser pulse at various fluences ( $\sim 6 \times 6 \mu\text{m}^2$  area). The images of the samples prepared at fluence of  $27 \pm 0.7 \text{ mJ/cm}^2$ ,  $30 \pm 0.7 \text{ mJ/cm}^2$ , and  $38 \pm 0.7 \text{ mJ/cm}^2$  ( $\sim 5 \times 5 \mu\text{m}^2$  area) are shown in (a), (b), and (c), respectively. The corresponding depth profiles are depicted in (d).



**Figure 6.** A cross-sectional TEM image of an a-AlO<sub>x</sub> sample treated with 35±0.7 mJ/cm<sup>2</sup> fluence. A typical pit is seen here, of ~200 nm width and 3-4 nm depth. A crystallized area is recognized in the AlO<sub>x</sub> beneath the centre of the pit.

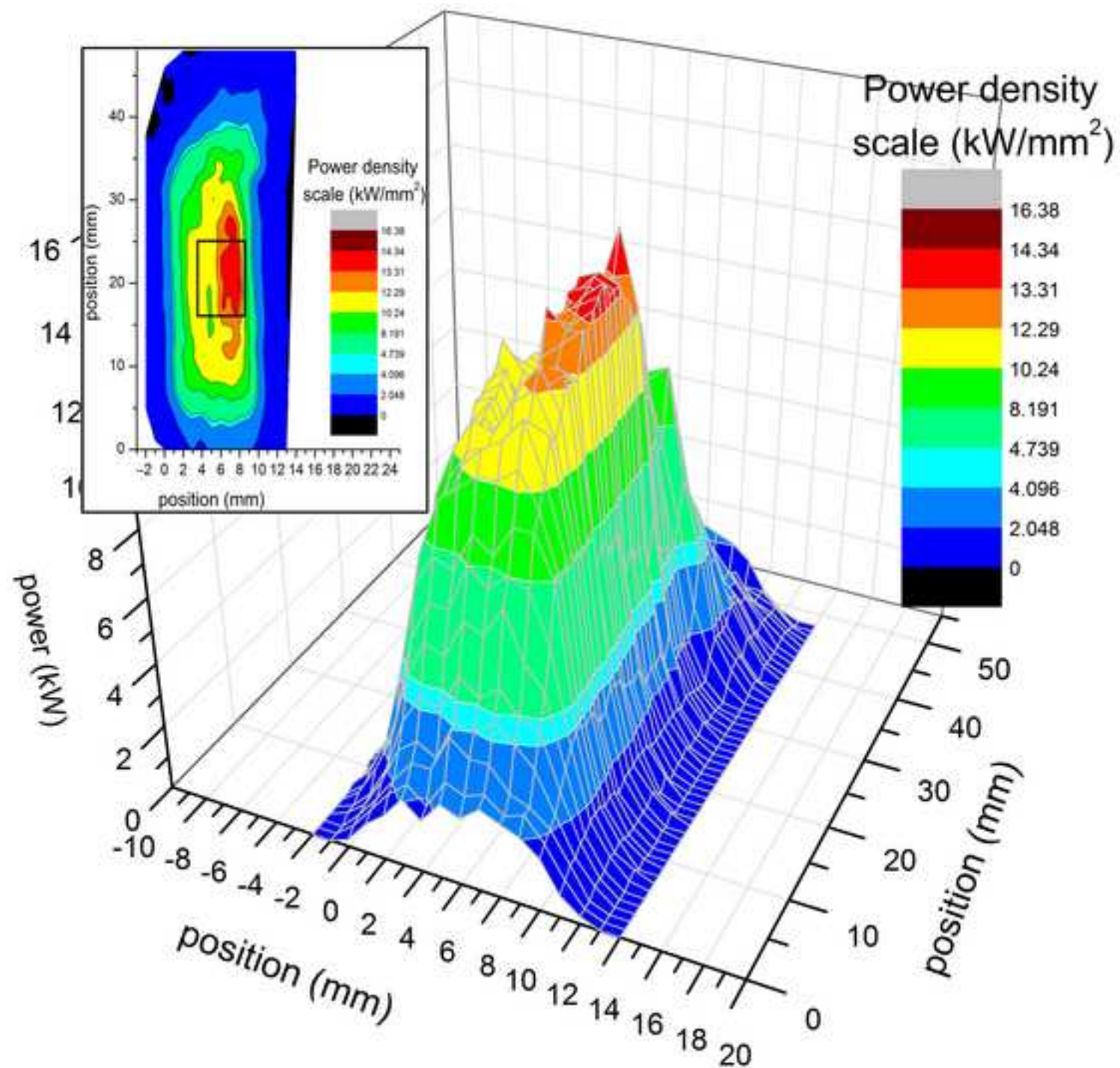
**Figure 7.** AFM image of an a-AlO<sub>x</sub> sample prepared at 30±0.7 mJ/cm<sup>2</sup> laser fluence, demonstrating the size (at least 80x80 μm<sup>2</sup>) of a patterned area. The arrangement and perfection of the pit pattern is directly related to that of the applied layer of silica nanospheres. Inset: a magnified ~9x9 μm<sup>2</sup> area.

**Figure 8.** AFM image of a pattern of hillocks, bubbles and burst bubbles obtained at a fluence of 32 mJ/cm<sup>2</sup> in a nc-Al/AlO<sub>x</sub> film. Inset: a magnified ~2.5x2.5 μm<sup>2</sup> area.

**Figure 9.** Side view TEM images of a hillock (a), a blown up bubble (b) and a burst bubble (crater) (c) formed in nc-Al/AlO<sub>x</sub> layers at the focal points of silica nanospheres under slightly increasing laser fluences. The average fluence was 32 mJ/cm<sup>2</sup>.

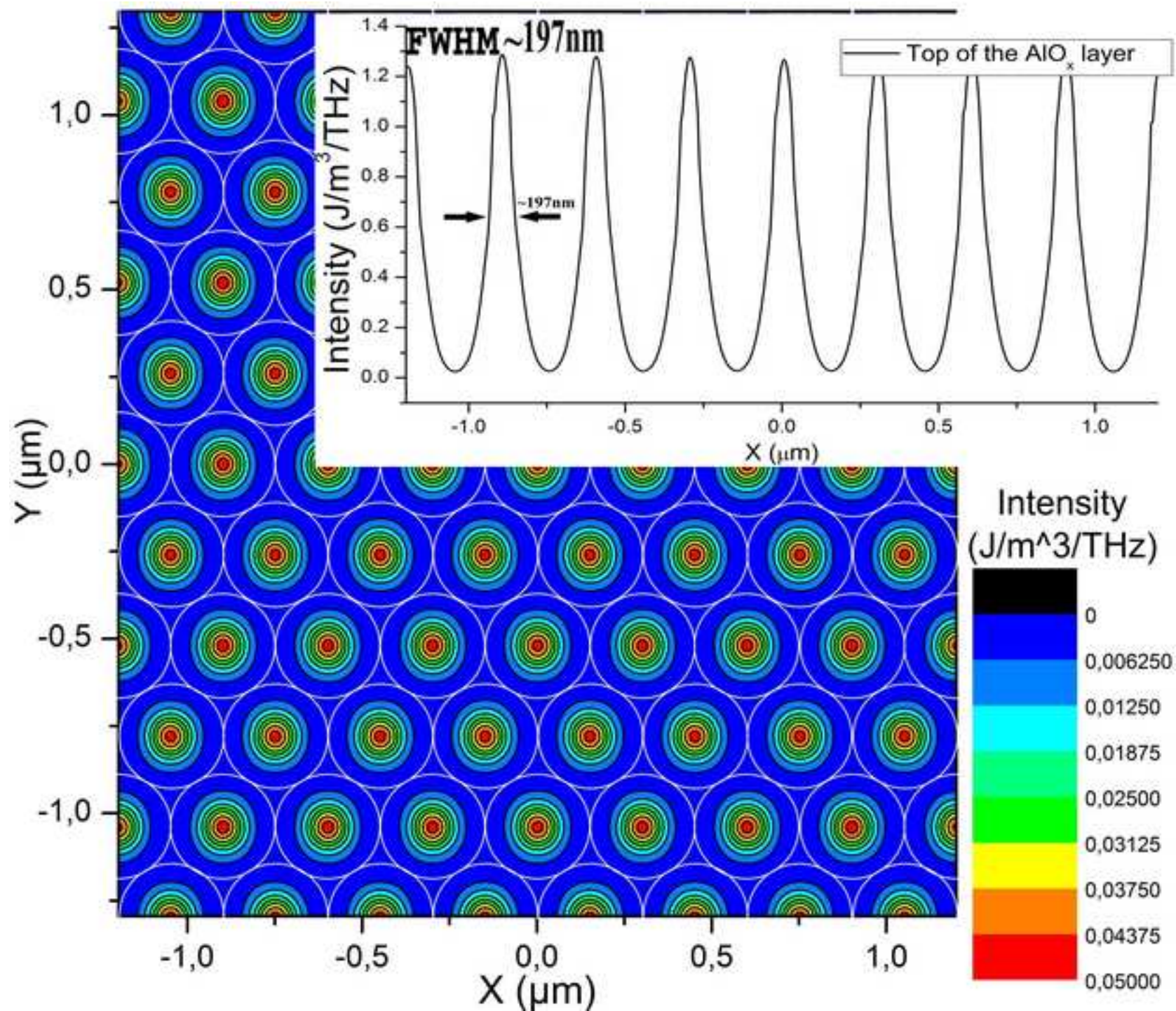
Figure

[Click here to download high resolution image](#)



Figure

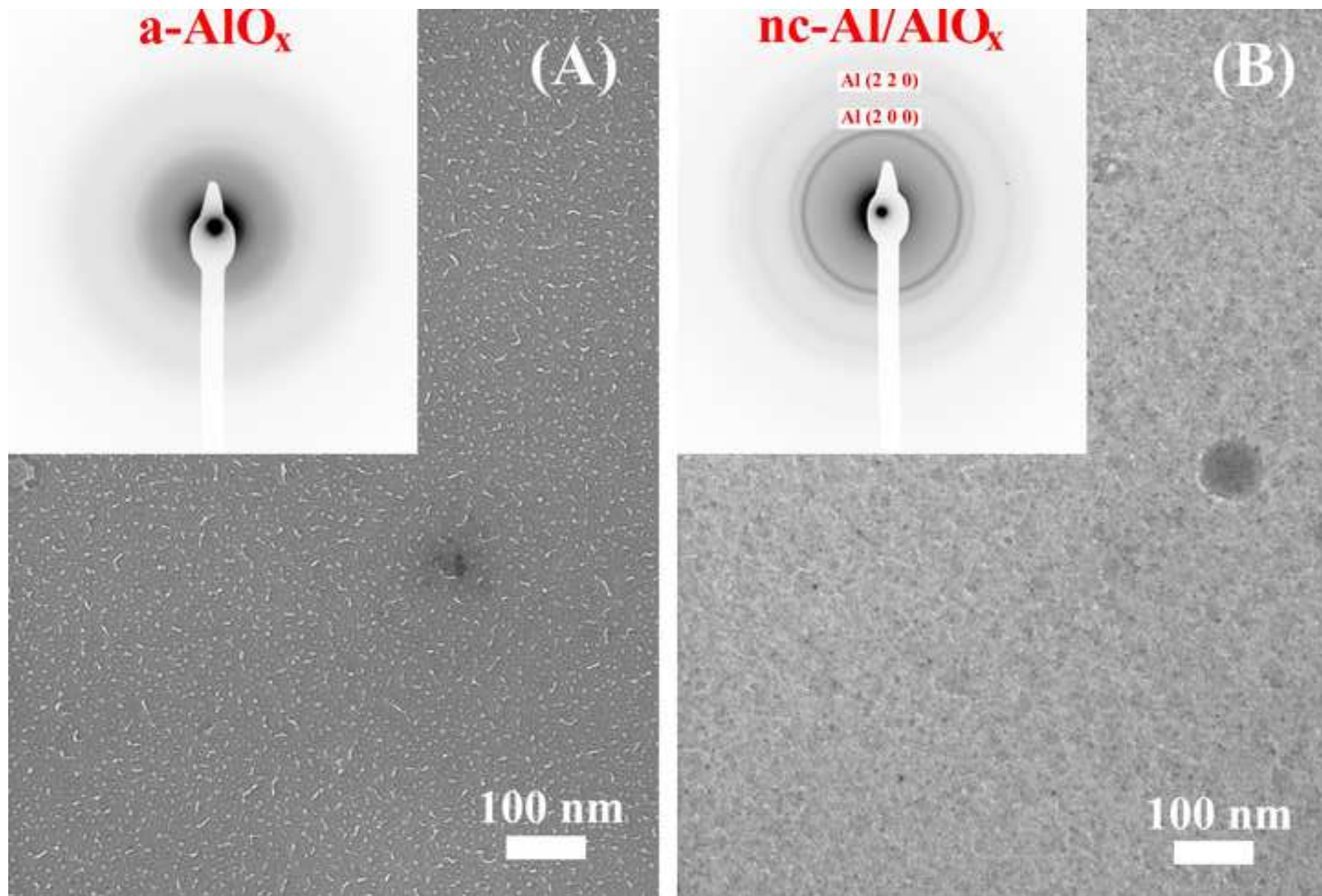
[Click here to download high resolution image](#)





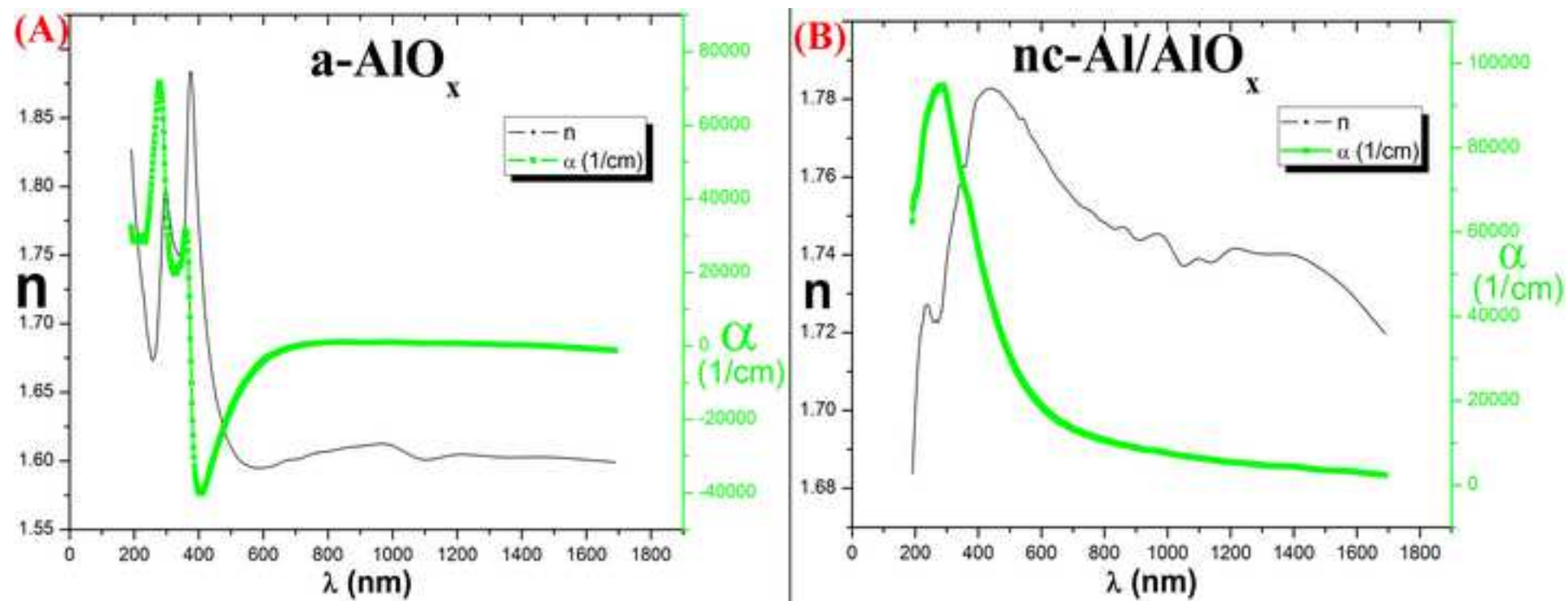
Figure

[Click here to download high resolution image](#)



Figure

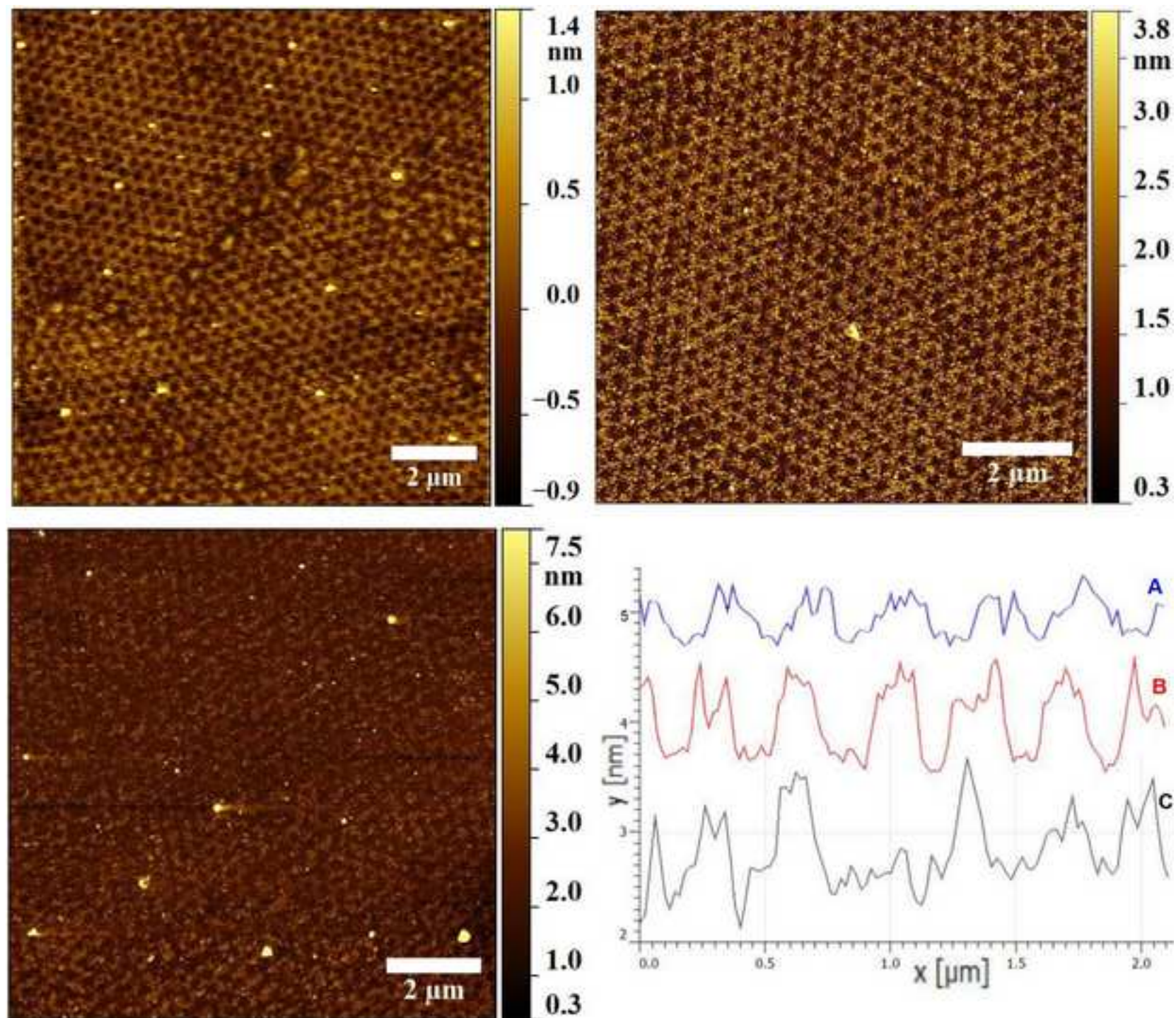
[Click here to download high resolution image](#)





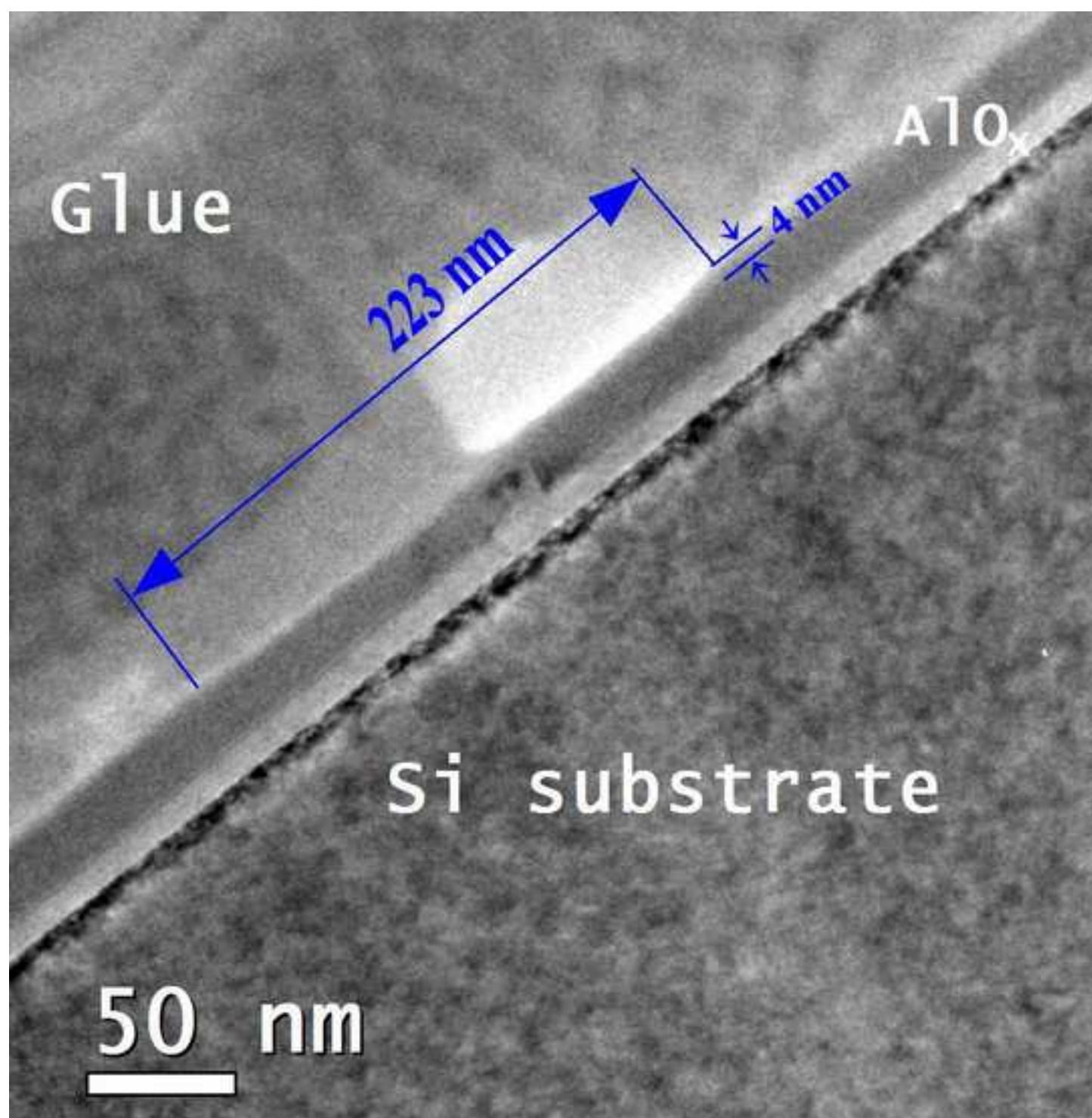
Figure

[Click here to download high resolution image](#)



Figure

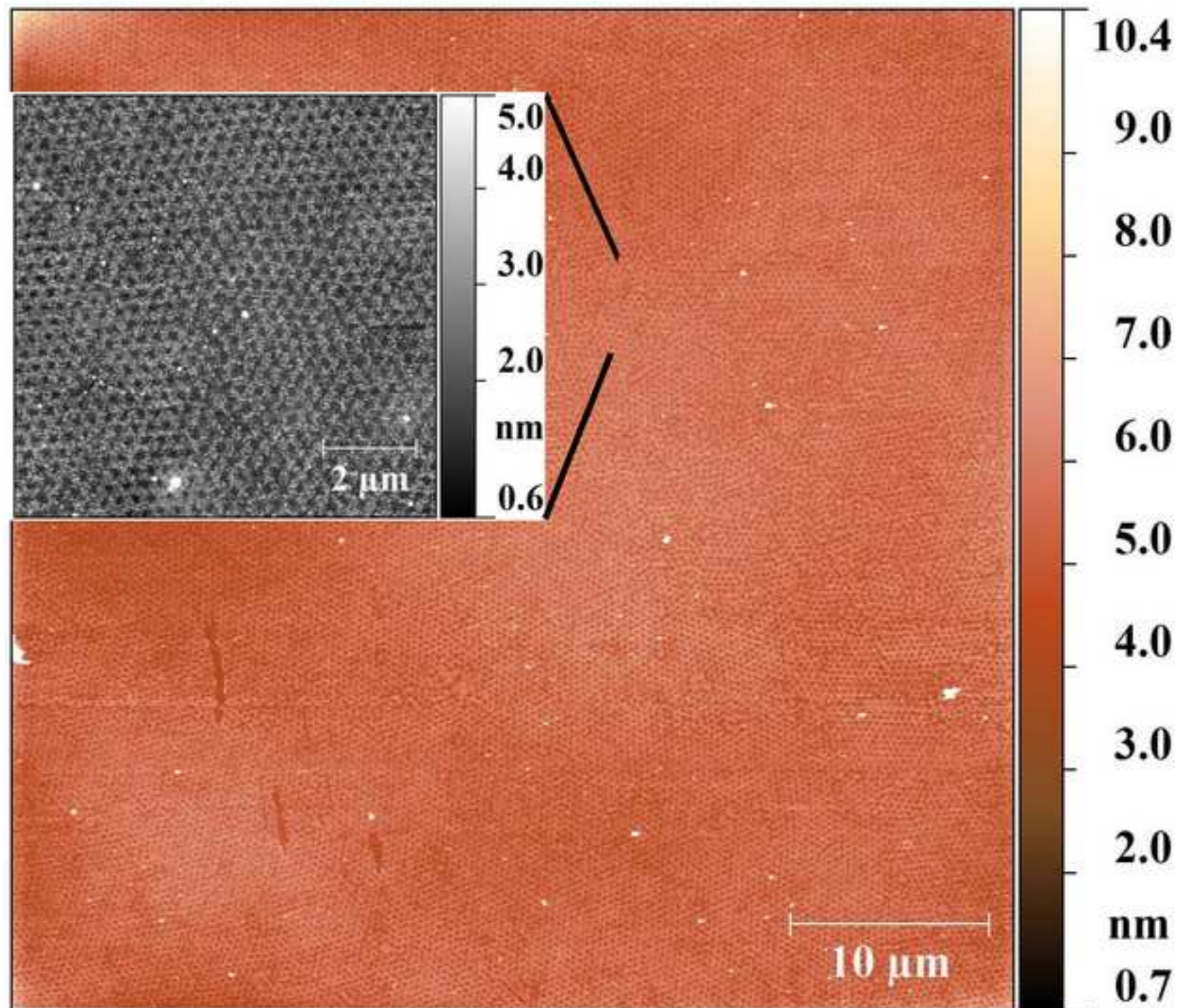
[Click here to download high resolution image](#)





Figure

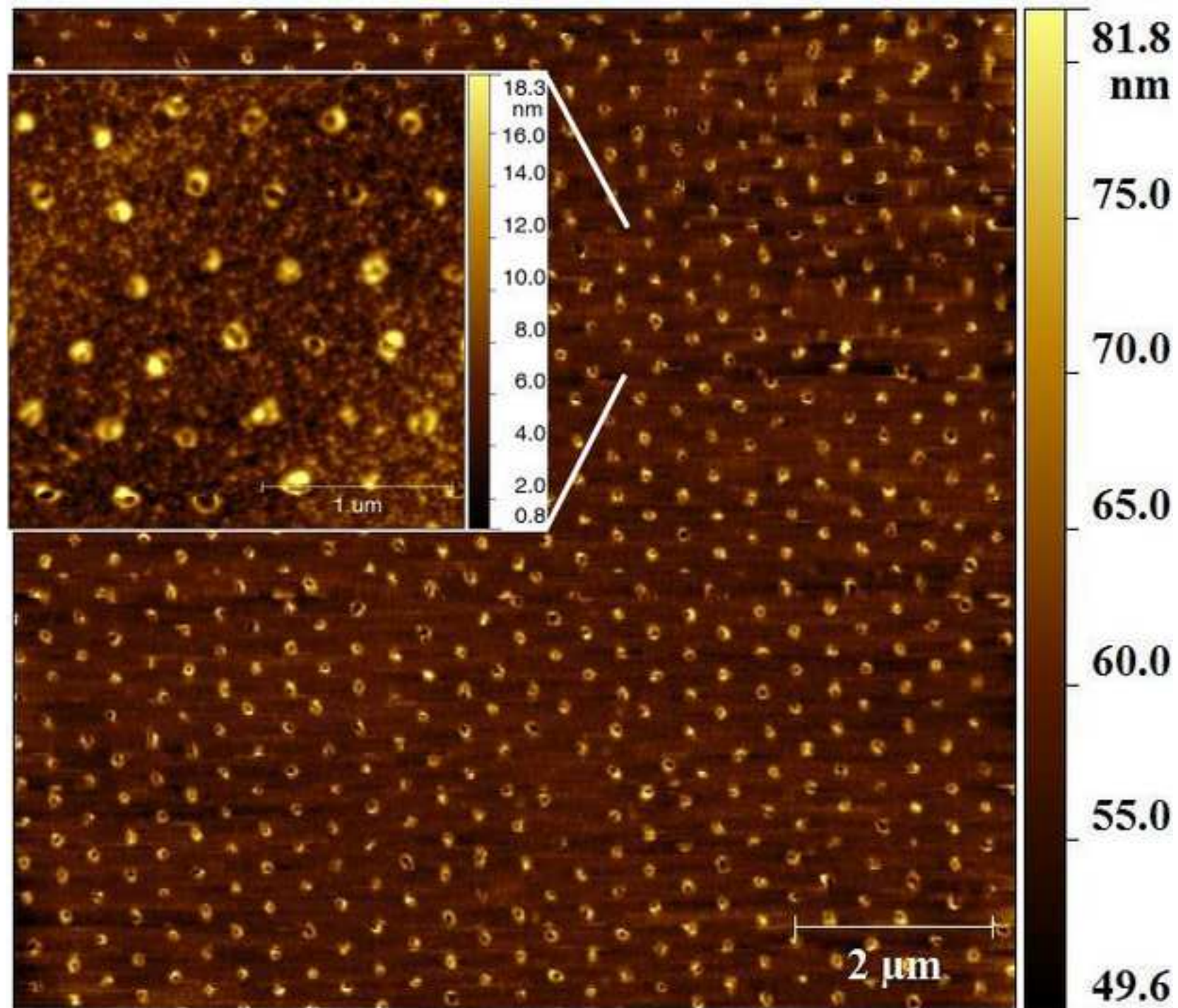
[Click here to download high resolution image](#)





Figure

[Click here to download high resolution image](#)



Figure

[Click here to download high resolution image](#)

